Continuous Fading Suppression Method for Φ-OTDR Systems Using Optimum Tracking Over Multiple Probe Frequencies

Mohammadmasoud Zabihi, Yusheng Chen, Tong Zhou, Jingxiao Liu, Yuanyuan Shan, Zhen Meng, Feng Wang, Yixin Zhang, Xuping Zhang, and Mengmeng Chen

***Abstract*—The demand for distributed acoustic sensors, which are capable of reconstructing the amplitude, frequency, and phase of an acoustic field, is increasing. These sensors are typically realized by phase-sensitive optical time-domain reflectometry (Φ-OTDR). However, common Φ-OTDR systems suffer from a fading phenomenon, which causes amplitude fluctuation on Rayleigh backscattering traces, and the scattered light may not have enough intensity in some regions. These areas have low amplitude backscattering that may be even lower than the system noise floor during some periods of time. Therefore, we cannot reconstruct the phase signal properly in such low intensity areas. Systems with multiple frequencies have been proposed to achieve fading suppression. However, online data processing of such schemes remains a challenge, especially for continuous in-field applications. Prediction of fading must be performed in real time. Any delay caused by massive calculations is not acceptable. In this paper, a continuous fading suppression method based on a Φ-OTDR system with three different probe frequencies is presented as well as a tracking algorithm for selecting the optimum probe signal for any time, which predicts the occurrence of fading before it actually occurs. The performance of the proposed method has been experimentally evaluated and statistically analyzed. The distortion induced by the fading effect could be suppressed to 1.15% under continuous real-time running. The method is highly effective and repeatable, which makes it suitable for practical online purposes.**

***Index Terms*—Fading effect suppression, multi-frequency, optimum-tracking, phase-sensitive optical time domain reflectometry (Φ-OTDR).**

I. Introduction

UNLIKE conventional sensors that measure a single position, distributed optical fiber sensors can detect measurements all over the fiber. In recent years, there has been a growing interest in distributed acoustic sensors (DASs), which are capable of reconstructing the full vector field, namely the amplitude, frequency, and phase, of an acoustic event. Using Rayleigh backscattering (RBS) light waves in optical fibers is one of the major techniques in DAS systems. This kind of system injects probe light into the fiber and measures the phase changes of the RBS that result from random inhomogeneities that are inevitably formed during the manufacturing procedure. For each location along the fiber, the phase of the scattered light is specific to the location and to the carrier frequency of the probe pulse. [1] The RBS based DAS is commonly realized by a phase-sensitive optical time domain reflectometry (Φ-OTDR) scheme, which originates from OTDR but utilizes a highly coherent laser as the light source. This technology has been widely used in many applications, such as structure health monitoring, intrusion detection, underwater acoustics, and seismic monitoring. However, Φ-OTDR has the problem of fading, which causes amplitude fluctuation on RBS traces. The origin of fading is commonly considered the random nature of RBS, which results in a speckle-like phenomenon. In many Φ-OTDR systems, the coherent optical backscattering power changes by a factor of 1000 in a fiber under test (FUT). When the intensity of the backscattered light drops into the fading areas, the signal-to-noise ratio (SNR) is not good enough to achieve valid signal demodulation, leading to a high rate of false events [1]. Healey *et al.* determined that the speckle-like phenomenon cannot stationary occur because of the random behavior of inhomogeneous scattering and laser source instabilities. The fading can be relieved by averaging various RBS traces over time directly or by a randomization process [2]. However, because the unintentional distributions of strains and temperature along the fiber are spatially random but relatively temporally stable, the fading cannot be vanished

Manuscript received February 3, 2019; revised April 8, 2019 and May 17, 2019; accepted May 19, 2019. Date of publication May 22, 2019; date of current version July 15, 2019. This work was supported in part by the National Natural Science Foundation of China under Grant 61627816, in part by the Key Research and Development Program of Jiangsu Province under Grant BE2018047, in part by the Natural Science Foundation of Jiangsu Province under Grant BK20180328, in part by the Fundamental Research Funds of the Central Universities under Grant 021314380095, Grant 021314380136, and Grant 021314380116, and in part by the Chinese Scholarship Council under Grant 2017GXZ022724. *(Corresponding authors: Yixin Zhang, Xuping Zhang, and Mengmeng Chen.)*

M. Zabihi, T. Zhou, J. Liu, Y. Shan, and F. Wang are with the Key Laboratory of Intelligent Optical Sensing and Manipulation, Ministry of Education, China (e-mail: dg1734501@smail.nju.edu.cn; mg1734013@smail.nju.edu.cn; mg1834007@smail.nju.edu.cn; violet-shan@smail.nju.edu.cn; wangfeng@nju.edu.cn).

Y. Chen is with the Nanjing University of Science and Technology, Nanjing 210094, China (e-mail: chenyusheng@njust.edu.cn).

Z. Meng is with the Beijing University of Posts and Telecommunications, Beijing 100876, China (e-mail: zmeng@bupt.edu.cn).

Y. Zhang and X. Zhang are with the Key Laboratory of Intelligent Optical Sensing and Manipulation, Ministry of Education, China, and also with the Key Laboratory of Modern Acoustics, Nanjing University, Nanjing 210093, China (e-mail: zyixin@nju.edu.cn; xpzhang@nju.edu.cn).

M. Chen is with the School of Electronics and Engineering, Nanjing Xiaozhuang University, Nanjing 211171, China (e-mail: chenmm@njxzc.edu.cn).

Color versions of one or more of the figures in this paper are available online at http://ieeexplore.ieee.org.

Digital Object Identifier 10.1109/JLT.2019.2918353

by simply averaging over multiple scans with a fixed probe frequency.

One of the first methods to overcome fading was the frequency hopping technique using a laser source. This method changed the laser frequency gradually by changing the temperature and the backscattered signal integration. Although this technique could successfully reduce the amplitude fluctuation, it requires thousands or even tens of thousands of averages, which makes it unsuitable for online applications. In addition to the massive mathematical process, altering the temperature is not an accurate way of changing the central frequency. It also causes drifting in the state of polarization and can result in unexpected changes to the RBS light. This research mainly focused on OTDR designed for long-term submarine cable monitoring. However, the idea could be instructive for Φ-OTDR [3], [4].

Time-gated digital optical frequency domain reflectometry (TGD-OFDR) was used for an OFDR system. Although OFDR is targeted for the frequency domain, time-gated OFDR can be exploited as a DAS function. Researchers [5] used an intensity modulator, and it had a large modulation bandwidth. This modulator created both positive and negative frequencies that could be used to suppress fading. This method may be good for OFDR; however, in a heterodyne Φ-OTDR, negative and positive frequencies have the same beat signals, and it is difficult to separately demodulate them. However, one interesting application is to adopt the similar idea of time gating to Φ-OTDR systems [5]. The multi-frequency nonlinear frequency modulation (NLFM) optical pulse is another method to suppress fading. This method produces a CW light with nonlinear tuning frequencies. In this method, the light pulse first was boosted, and then RBS was compressed to suppress the optical nonlinear effects. This compression occurred during signal processing to obtain higher probe pulse energy without sacrificing the spatial resolution. Then, the overall SNR increases, which reduces the probability of fading. However, for long-distance measurements, when the RBS intensity attenuates in the far end of the sensing fiber, fading is still a problem [6].

By injecting independent frequencies into the probe light, the fading phenomenon all through the FUT could possibly be avoided because the location of fading areas are different for independent probe frequencies [1], [7]. It has been confirmed that the location of fading points varies with the drifting of the central frequency of the laser [8]. Therefore, a simulated model has been proposed that considers the propagation phase factor and multiplies it with a random Gaussian distributed scattering coefficient. The simulation was only calculated for 40 msec; thus, the longtime evolution of fading has not been studied [9]. Hartog *et al.* studied the amplitude and SNR enhancement for a seismic sensing system using multiple probe frequencies. They aggregated the data obtained to substantially reduce the noise caused by fading. As well as reducing the effects of fading, the aggregation of the independent results also helped to reduce the overall noise of the measurement and improve the linearity of the distributed vibration sensing system. However, in the case of seismic waves, it does not require a long sensing time, and the incoming perturbation only lasts for a few seconds. Therefore, they did not have the problem of dynamic selection of probe frequencies. Moreover, they focused more on the fading effect suppression for the amplitude, and the phase signal behavior in the fading zones was not discussed [1]. In all these studies, fading suppression has only been performed for a very short time, whereas the RBS for a given region proceeds to fading state and comes out of it very slowly but continuously. Therefore, the monitoring time must be at least several hundreds of seconds to provide enough time to all scattering regions to experience fading several times.

In this paper, we present a practical continuous fading suppression method that can reconstruct the phase signal with a high accuracy. We utilized a coherent Φ-OTDR system with three independent frequencies, which is supported by an optimum-tracking algorithm that can predict the fading phenomenon and chooses the optimum probe frequency that provides the best phase signal for each moment. This method was experimentally tested on a very long recorded dataset, which could continuously suppress the fading phenomenon, and it has the desired output phase signal.

II. Principles of Phase Demodulation Over Multiple Frequencies

In a heterodyne Φ-OTDR system, the photocurrent, i_{het}, of a photodetector after bandpass filtering can be expressed as [10]:

$$i_{het} = 2E_{lo}E_b \exp\left[\mathrm{j}\left(\Delta\omega \mathrm{t} + \Phi\ (\mathrm{t})\right)\right] \tag{1}$$

where E_{lO} is the electric field of the optical local oscillator, E_b is the electrical field of RBS light, $\Delta\omega$ is frequency shift provided by a modulator, and $\Phi(t)$ is the phase of the RBS. We can simplify it to:

$$i_{het} \propto E_0 \cos\left(\Delta\omega \mathrm{t} + \Phi\left(\mathrm{t}\right)\right) \tag{2}$$

where E_0 is the magnitude of the electric field. The changes in backscattered phase signal are highly nonlinear [7]. Therefore, in vibration sensing applications, it is common to use the phase difference between two specific points. For each location along the fiber, the amplitude and phase of the scattered light are specific to the location. We can observe any zone along the fiber by selecting reference sections before and after that area and analyze the relative phase changes between them. When observing an area with a length of *L*, we can consider having two regions, such as *A* and *B* (Fig. 1), to compare the phase difference between the backscattered light from the two sections [7]. Regardless of fiber loss, the backscattered electric field from *A* and *B* at the photodetector is given by:

$$E_A = E_0 \mathrm{Cos}[(\Delta\omega t + \Phi_A)] \tag{3}$$

$$E_B = E_0 Cos\left[(\Delta\omega t + \Phi_B)\right] \tag{4}$$

Fig. 1 shows how an external perturbation that induces extra stress on the fiber and results in a change in length. The change in length is directly related to the change in relative phase between the two regions. Any external perturbation within two specific points changes the phase of the backscattered light [11].

$$\Delta\Phi = \frac{4\pi n}{\lambda}\Delta L \tag{5}$$

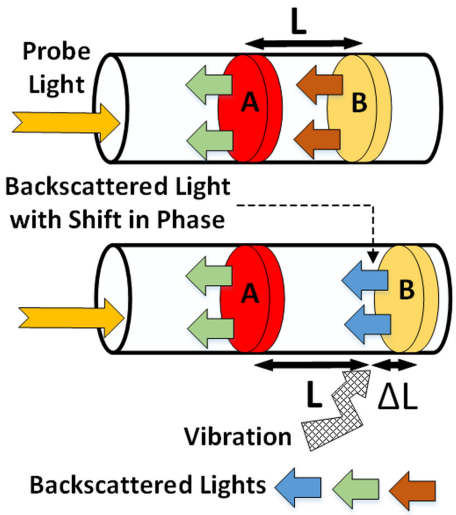

Fig. 1. Principles of dynamic strain and its influence on the phase before and after vibration.

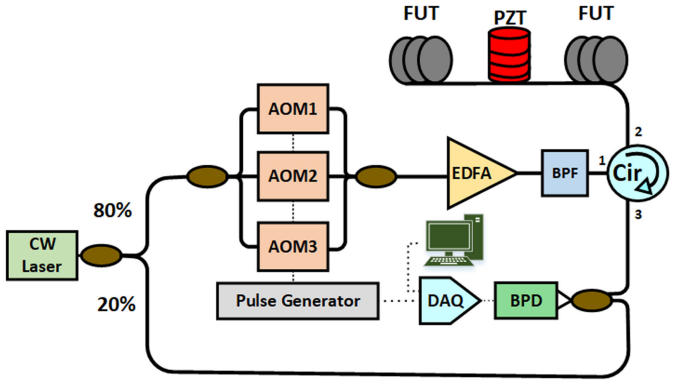

Fig. 2. System setup. CW Laser: Continuous Wave Laser; AOM: Acousto-Optical Modulator; EDFA: Erbium-Doped Fiber Amplifier; BPF: Bandpass Filter; Cir: Circulator; FUT: Fiber Under Test; PZT: Piezo-electric Transducer; BPD: Balanced Photo Detector; DAQ: Data Acquisition Card.

Here, n is the refractive index of the fiber, and λ is the wavelength of probe light. Any disturbance event that occurred within the two points can be monitored by demodulating the phase difference change, $\Delta\Phi$.

Because bandpass filtering is used to extract each beat frequency, the in-band noises in our system inherit the same frequency, $\Delta\omega$, as the beat signal. If we consider the noises of active devices as broadband white noises and we bandpass them, then we can rewrite the output photocurrent as

$$i_{het+Noise} = K\cos\left(\Delta\omega t + \phi_{(t)}\right) + N\cos\left(\Delta\omega t + \phi_n(t)\right) \tag{6}$$

where K is the amplitude of the backscattered signal, N is the random noise amplitude, $\phi(t)$ is the phase of RBS, and $\phi_n(t)$ shows the phase of the noise signal. Because we bandpassed the white noise after the photodetector, we can expect the distribution of the noise amplitude, N, to be Gaussian and the distribution of the noise phase, $\phi_n(t)$, to be uniform. We exploited an *I/Q* demodulation system [12]. After lowpass filtering, we have two terms in the form of

$$\begin{cases} i_I = \frac{K}{2}\cos\left(\phi_{(t)}\right) + \frac{N}{2}\cos(\phi_n\ (t)) \\ i_Q = \frac{K}{2}\sin\left(\phi_{(t)}\right) + \frac{N}{2}\sin(\phi_n\ (t)) \end{cases} \tag{7}$$

The phase of the backscattering signal can then be obtained by:

$$\Phi_{total} = \tan^{-1}\frac{\frac{K}{2}\sin\left(\phi_{(t)}\right) + \frac{N}{2}\sin(\phi_n\ (t))}{\frac{K}{2}\cos\left(\phi_{(t)}\right) + \frac{N}{2}\cos(\phi_n\ (t))} \tag{8}$$

Equation (8) shows how vulnerable the phase demodulation output is to noise. If the random noise term becomes high, the arctangent changes and extracted phase signal will experience a significant inaccuracy. Even a noisy signal from one of the two positions for phase demodulation can affect the output. If φ'_A and φ_A are the demodulated phase value (including noise) and the desired phase value in region A, respectively, and if φ'_B and φ_B are the demodulated phase value (including noise) and the desired phase value in region B, we can write:

$$\begin{cases} \varphi'_A = \varphi_A + \varphi_{NA} \\ \varphi'_B = \varphi_B + \varphi_{NB} \end{cases} \tag{9}$$

where φ_{NA} and φ_{NB} are added phase noise values.

$$\begin{cases} \Delta\varphi = \varphi_A - \varphi_B \\ \Delta\varphi' = (\varphi_A - \varphi_B) + (\varphi_{NA} - \varphi_{NB}) \end{cases} \tag{10}$$

Similarly, $\Delta\varphi$ is the phase difference that we are looking for, whereas $\Delta\varphi'$ is what we can practically obtain at the output. If the received signal from either A or B does not have a good SNR, the $\Delta\varphi'$ term would not carry valid information about the applied perturbation.

According to previous studies and our own experimental results [1], [7], [13], a change in the optical frequency of the probe pulse changes the phase of the RBS from each region, such as A or B. It means that if there is fading in either A or B for one probe frequency, the RBS may actually be quite strong at a different frequency. However, these various probe frequencies must be selected properly to have minimum possible phase correlation [13]. To remove the phase correlation between every two frequencies and to have independent probe lights, different frequencies must satisfy:

$$\Delta f = f_2 - f_1 \geq v_g/4L \tag{11}$$

where f_1 and f_2 are the frequencies of the probe light, v_g is the group velocity in the fiber, and L is the physical distance between A and B (gauge length).

III. Experimental Setup

The proposed method exploits the changes in fading regions to mitigate the fading phenomenon. The optical arrangement for a Φ-OTDR-based vibration sensor with multiple probe frequencies is shown in Fig. 2. The output of a CW laser with frequency ω_0 (1550 nm, RIO ORION laser module) is split into a local oscillator and sensing paths. Regarding equation (11) and considering L = 30 m, we need at least a 1.66 MHz difference between nearby frequencies to consider them independent. In this case, we use a 100 ns pulse width, and it covers 10 m in FUT, and L =

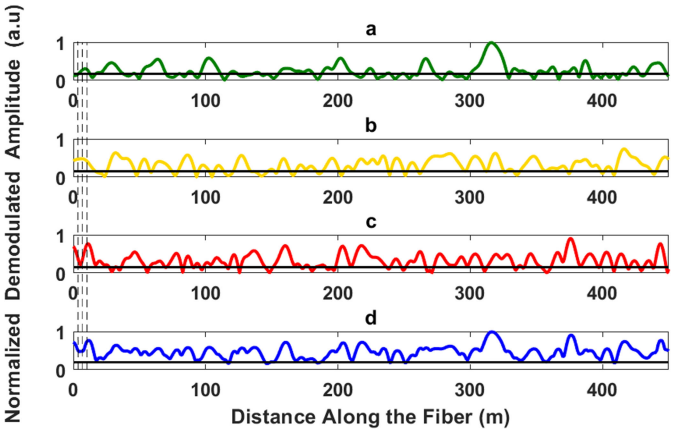

Fig. 3. Demodulated amplitudes on 450 m of fiber. a: 40 MHz, b: 80 MHz, c: 150 MHz, d: Maximum value for each chosen section between dashed lines. The horizontal black line shows the threshold. The vertical dashed lines are spatial sections.

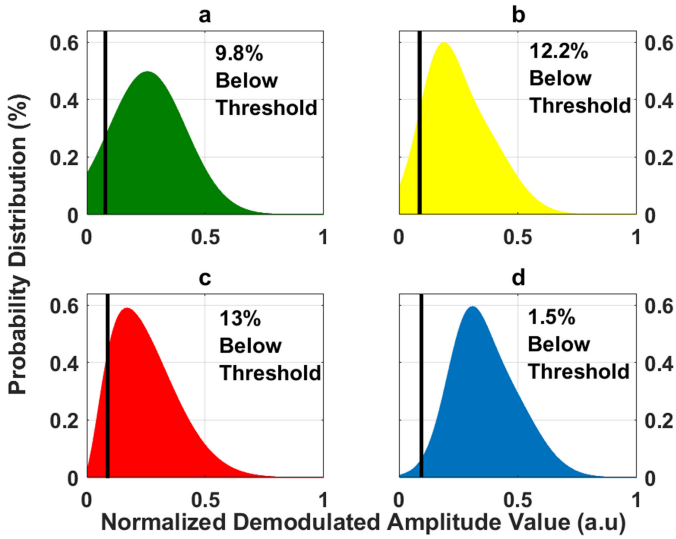

Fig. 4. Probability distributions (all recorded data) for a: 40 MHz, b: 80 MHz, c: 150 MHz, d: Maximum values for each chosen section. The vertical black line shows the threshold.

30 m meets this criterion. Three acousto-optic modulators create a probe pulse and shift their frequencies by 40 MHz, 80 MHz and 150 MHz ($\Delta\omega\_1$, $\Delta\omega\_2$, $\Delta\omega\_3$, respectively). These three pulses are synchronized with each other, and all pulses have a 100 ns width with a 1 kHz repetition rate. After amplification in an erbium-doped fiber amplifier, the probe pulses are launched into the FUT through a circulator. The first piece of fiber is 450 m, followed by a 30 m cylindrical PZT actuator, which is stimulated with a 25 Hz sinusoidal wave. Then, a 1079 m fiber is located on the far end of the FUT. The RBS returning from the FUT at frequency $\omega_0 + \Delta\omega$ is mixed at the receiver with the OLO, resulting in three intermediate frequencies. A balanced photodetector with a 200 MHz bandwidth converts the optical signal to an electrical signal. An 8-bit data acquisition system is used to capture the output data with a 1 GHz sampling rate. A pulse generator synchronizes all three AOMs and the data acquisition system.

IV. Amplitude Distribution for High-Risk Areas

The RBS amplitude level changes from section to section because the distribution of scatterers is not uniform along the fiber, and it follows Rayleigh statistics [2]. After bandpass filtering and IQ demodulation, each demodulated frequency would have many low amplitude regions, which may cause fading, as shown in Fig. 3 (a, b, c). We considered a threshold to add to our plots, which could guarantee at least a 10 db SNR at the output for areas above it. If we divide our outputs into several sections (like the dashed lines on the left side of Fig. 3) and choose the signal that has the highest amplitude in each section as the output signal (Fig. 3(d)), we can reduce the number of low SNR areas. In Fig. 3, 450 m of the FUT is shown. The blue figure barely but always remains on the top of the predefined threshold and stays away from the dead zones, while single frequencies fall into dead zones several tens of times. Nevertheless, the positions of the low amplitude points for each frequency are different from the others. When we statistically analyzed the amplitude values in the demodulated traces, we obtained the probability distribution shown in Fig. 4. In Fig. 4(a, b, and c), the peak point in the figure tends to the left side for every single frequency. Considering the 10 db threshold, more shifting to the left in the bell-shaped figures means more areas fall below the threshold and have a risk of fading. However, by selecting the highest curve in each section, we can shift the bell curve to the right, and a smaller portion falls below the threshold. Figure 4 shows a comparison of the probability distribution for all frequencies and the maximum value for each chosen section. The percentages of points below the threshold for 40 MHz, 80 MHz, and 150 MHz were 9.8%, 12.2%, and 13%, respectively. These decreased significantly to 1.5% in Fig. 4d corresponding to the maximum values for each spatial section. The small percentage shown in the last figure is related to the points where all three frequencies fall into the fading region simultaneously.

V. Optimum-Tracking Algorithm for the Best Phase Signal

If we consider the incoming data as a matrix, each row is an independent trace from the FUT, and each column corresponds to one point at different times. The time difference between every two consecutive rows is equal to the repetition period of incoming light pulses. Figure 5 was made from 100 consecutive traces in a specific part of the FUT. Each vertical line shows amplitude changes of a specific point within 100 msec, and each horizontal line shows the amplitude of all points in this 70 m of FUT during one probe pulse sweep. We averaged the columns corresponding to positions A and B separately for w consecutive traces. Column A shows the amplitude changes in position A with w arrays. Similarly, column B shows the amplitude changes in position B with w arrays. For every single beat frequency, we used these two mean values as the main parameters in our prediction model. A and B can be shifted

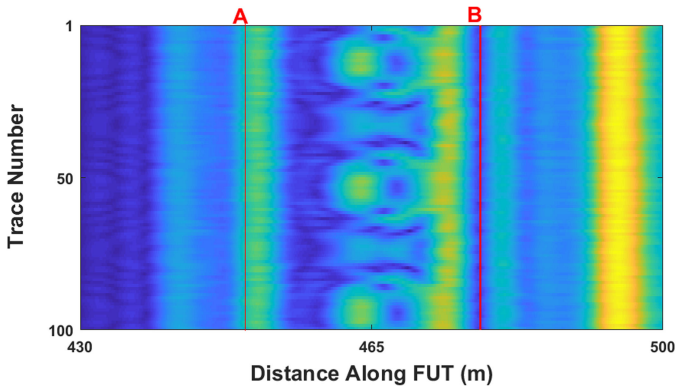

Fig. 5. Two points of phase demodulation sliding through the fiber (A and B). Each red line refers to one column corresponding to A and B.

along the FUT to determine the vibration zone; however, the distance between them must meet the requirements of equation (11). In Fig. 5, we put A and B on two sides of the PZT to retrieve the induced vibration signal correctly from our phase signal.

Figure 6, shows the phase differences of the same locations on two sides of the gauge for two different time ranges, a and b. During these given time ranges, we observed amplitude variations on both sides of the gauge as shown in Fig. 6(a). During this time, the amplitude of the left side was almost zero, and we could find distortion in some parts of the extracted phase signal. Referring to equation (10), it confirms that having a low SNR on even one side of the gauge results in a distorted phase signal. However, in Fig. 6(b), both sides are shown to have reasonable amplitudes, and we successfully retrieved the applied sinusoidal vibration from the phase signal. Here, we proposed a method to predict the occurrence of a distorted phase shape (such as the phase signal in Fig. 6(a)) and a switching mechanism to jump to another RBS trace that has an optimum phase signal. In this method, we separately observed the amplitude of the demodulated signal for each frequency. The demodulated amplitudes have some small fluctuations, and for mitigating the effect of fluctuations, we used averaging. We considered two points for making the phase demodulation, for example, two sides of the PZT, A and B, in Fig. 5. Then, we averaged through the time for those two positions for a specific time window (specific number of traces). Figure 7 presents a flowchart of our optimum-tracking algorithm. Initially, we fed the demodulation results into the flowchart and defined A and B and the size of the averaging window. After performing averaging on A and B columns for each beat frequency, this results in two values, M_k1 and M_k2. As mentioned above, the amplitudes on both sides of the gauge must be high enough if a good demodulation result for the phase difference is desired. Thus, a quick evaluation of the quality of the amplitude is tricky.

Considering the logic operation of 'AND' between two Boolean variables, the result would be '1' only if the two variables are '1' simultaneously. The 'AND' can be represented by multiplication. Therefore, in the next step, we multiplied M_k1 and M_k2 to obtain the 'AND' result for each given frequency (Pr_ω_k). We compared these multiplication results (Pr_ω_k) to select the maximum (F_max) that indicated which probe frequency would have the best phase signal in upcoming traces. After each round of processing, the averaging window slid one trace down, and this process continued. After selecting the best signal for phase extraction, the remaining processes were similar to a normal Φ-OTDR system [8], [14]. The same processing was performed in every position all along the sensing fiber. To connect the phase demodulation results from different probe frequencies when jumping from one frequency to the other, we applied a highpass filter to remove the different offsets of the phase signal after subtraction and unwrapping the demodulation phase output for each probe frequency.

VI. Experimental Results

To test and evaluate our proposed algorithm, we continuously recorded data for 375 s. This long recorded data guarantees that the RBS signal from all regions has enough time to experience various possible states. Figure 8 illustrates the output of approximately 13 s with an averaging window of $w = 100$. The extracted phases from the 40 MHz, 80 MHz, and 150 MHz traces showed distorted figures for some time ranges. We achieved an optimal trace only by hopping from a distorted signal to a well-shaped one at the proper time before distortion actually occurred. The six circled areas in Fig. 8 show the controversial points, where the system needed to quickly switch from the ongoing output that was about to distort to another beat frequency, which was expected to have the best phase signal for upcoming traces. Before the first controversial point on the 40 MHz trace, the system predicted the distorted phase signal and jumped to the 80 MHz trace. After 0.9 s, the 80 MHz trace also became close to a fading area, and the system hopped to the 150 MHz trace. Approximately 1 s later, the system switched back to the 40 MHz trace because fading of the amplitude in the 150 MHz output phase had been forecasted. On the right side of Fig. 8, we observe three similar points, and again before each abnormal phase shape, our algorithm accurately predicted and hopped to a better phase signal. The three figures for Pr_ω_k showed that when every two highest amplitude curves collided and one of them had overtaken the other, our prediction signal reacted and switched to another beat frequency. Nevertheless, each extracted phase signal had a different phase offset, and to remove those offsets, we added a highpass filter that behaved like a differentiator. Therefore, we achieved changes in $\Delta\varphi$ but not in $\Delta\varphi$ itself. The changes in the extracted phase signal from the most recent output of the algorithm directly became attached to the previous one. Therefore, the final output was very smooth, shaped well and free of distortion, as shown in Fig. 6(b), where both sides of the gauge were out of the fading zone.

The entire recorded data was very long. Therefore, for statistical analysis, we split the entire time into five separated time ranges to pore over the system behavior over time. The probability of failure for the extracted phase signals related to each frequency is shown in Fig. 9 as well as the probability of failure for our proposed algorithm over three window sizes (1, 30, and 100).

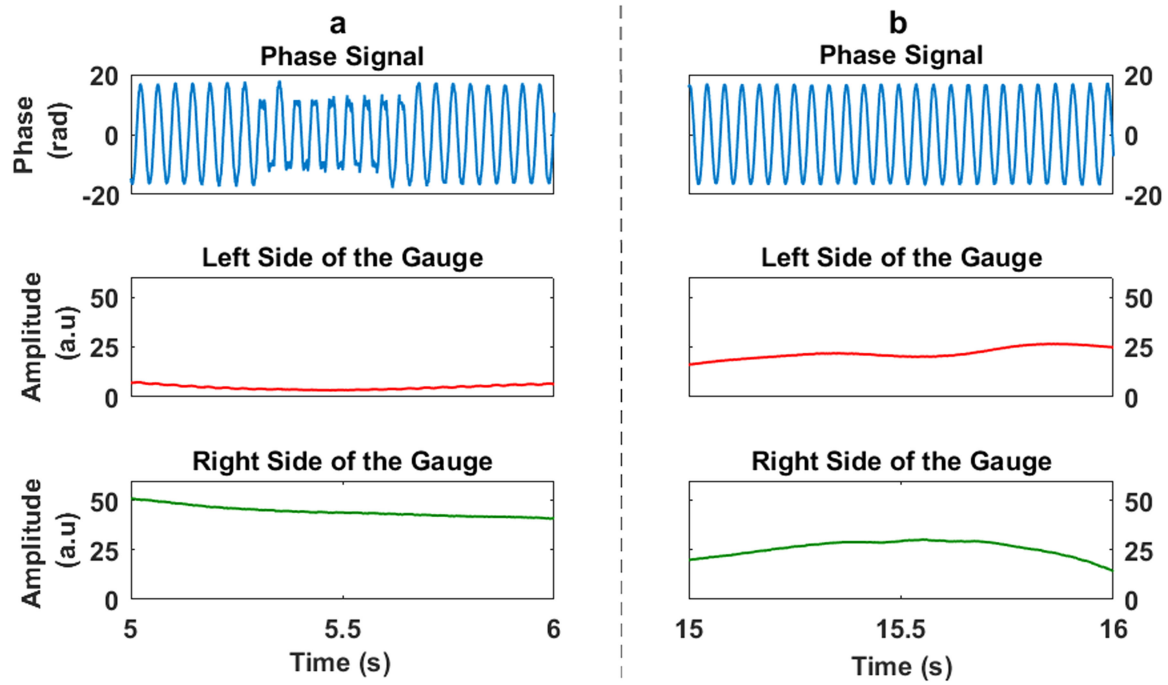

Fig. 6. Phase difference between two fixed points (gauge) within two different time ranges, a (5–6 s) and b (15–16 s). The variation in amplitude on both sides of gauge is also shown.

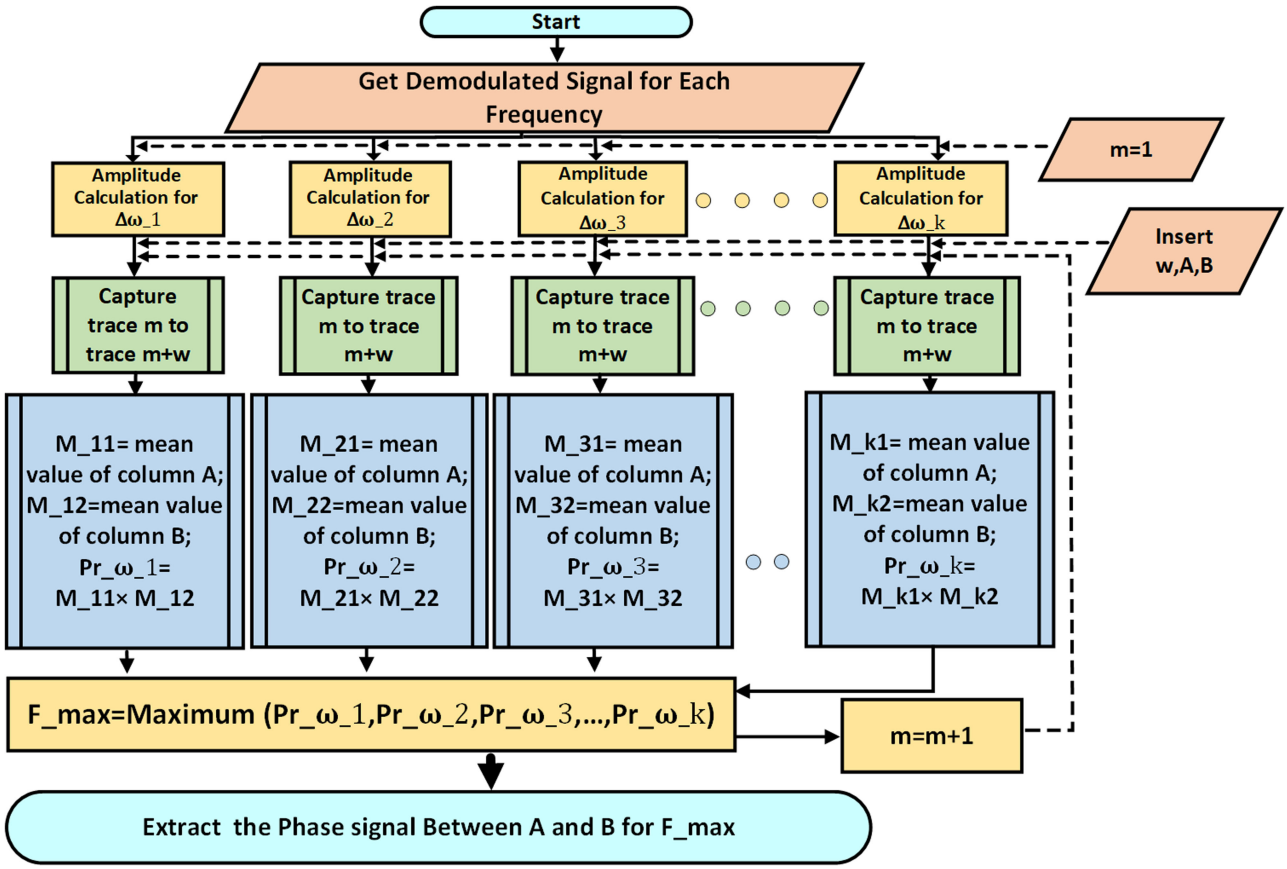

Fig. 7. Flowchart for predicting the best phase signal. w is the averaging window size, A and B are the locations for two sides of the gauge, k is the number of independent frequencies, and m is a counter.

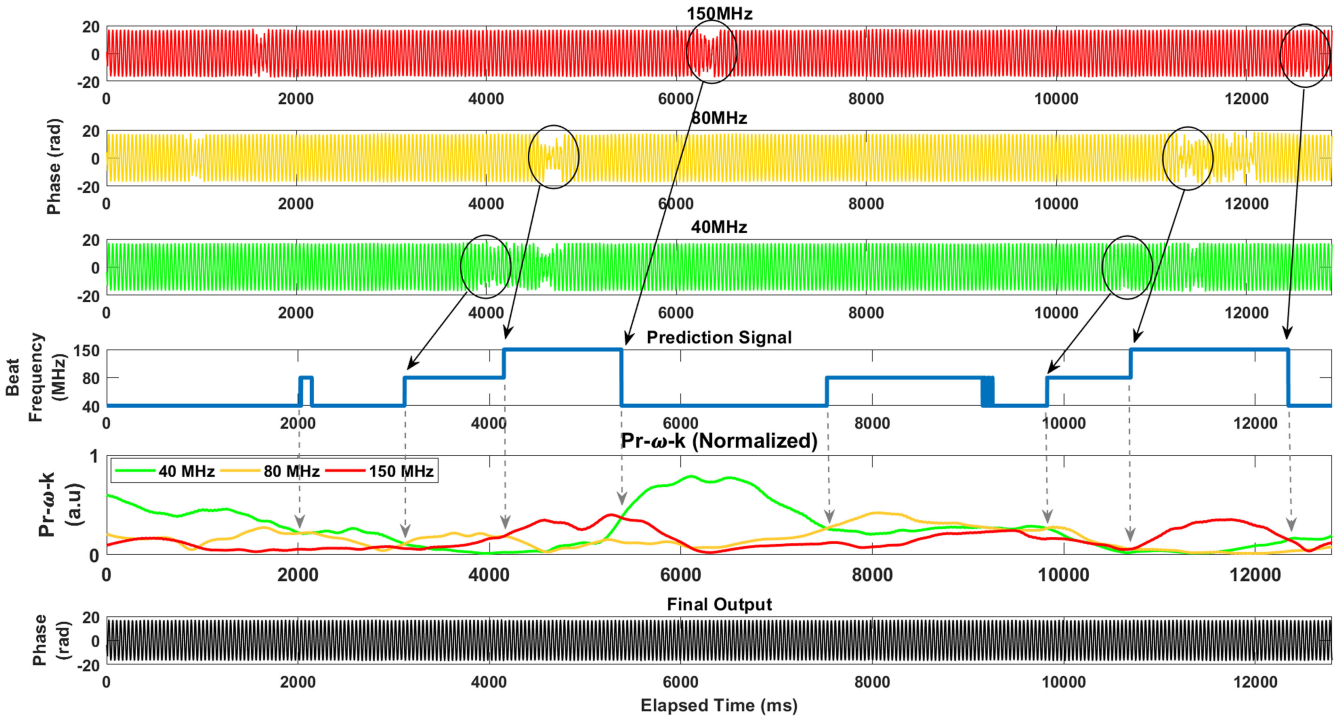

Fig. 8. Extracted phase signal from all single beat frequencies as well as the prediction signal and final output.

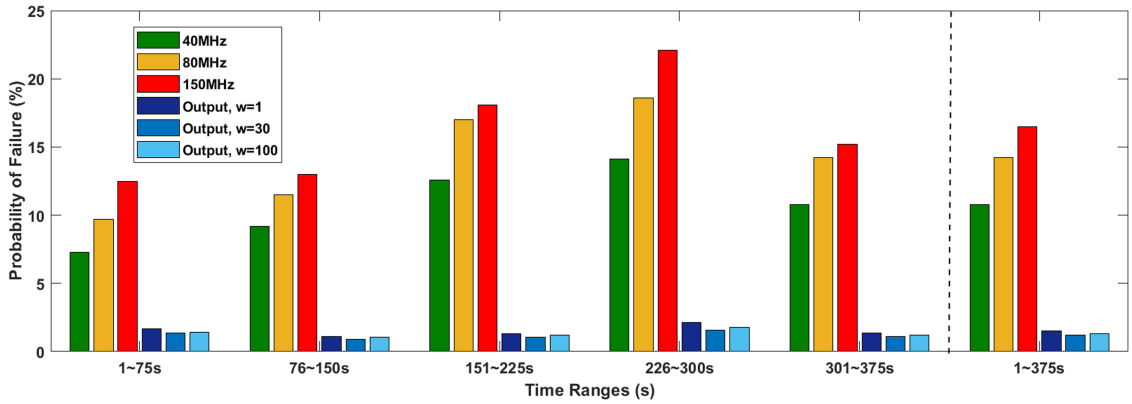

Fig. 9. System analysis as a function of time.

As shown in Fig. 9, the probability of having a distorted phase signal varied from 7% to 22%, while the proposed algorithm suppressed distortion areas to be approximately 1%. Although we observed different time ranges, in all cases, the probability of distortion in the final output phase had almost the same values, which confirmed that the system is highly repeatable. Moreover, the final output phase when $w = 30$ is slightly better than for $w = 1$ or $w = 100$. Among the three sole frequencies, 150 MHz always had the highest probability of distortion, and 40 MHz had the lowest. There are two main reasons for this behavior. First, the sampling rate of the data acquisition card was 1 GHz, which means that the beam with the 150 MHz frequency was rebuilt by less than 7 points during each period, whereas the one with 40 MHz was rebuilt by 25 points during each period. Second, the 3 db bandwidth of the balanced photodetector was 200 MHz, which means that the higher frequencies experience lower SNR at the output; thus, they are more exposed to fading phenomenon.

To further evaluation the impact of averaging window size on the proposed method, we presented the probability of failure or the entire data length for different window sizes (1–100) in Fig. 10. By increasing the window size, the probability of failure first decreased. The best result was obtained from $w = 32$, which was 1.15%. After $w = 32$, the probability slightly increased, but it stayed almost constant after $w = 50$. This was because although averaging reduces sudden fluctuations, the long averaging process prevents our system from reacting fast to the variation in RBS intensity itself. Consequently, the agility of the system declines, and the algorithm cannot predict distortions of phase signals with time, resulting in a poor output quality.

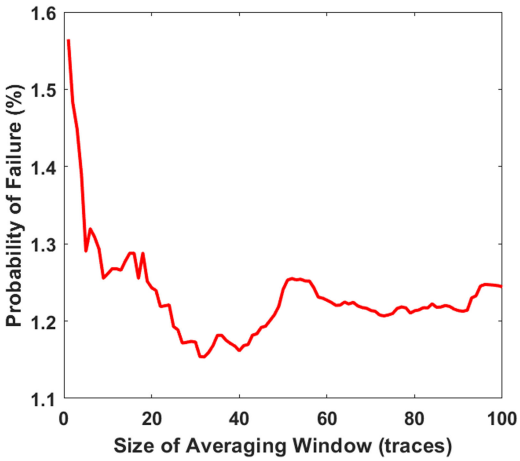

Fig. 10. Changes in probability of failure for different averaging windows.

Therefore, for the current setup, the optimum window was $w = 32$ (32 msec). Nevertheless, this value can change for another setup because it relates to the stability of the laser central wavelength, laser linewidth, changes in birefringence in the FUT and other in-field conditions. Selecting a proper window size is exactly like a calibration process. Because many different factors influence our system, we should first apply a known perturbation on our FUT and observe the window size that provides the best output. Then, we can use that window size for any further measurements in that environment and with that piece of fiber. For a given instrument and working environment, the proper window size would be approximately invariable.

Additionally, we had a 1 KHz repetition rate; thus, each new trace appeared after 1 msec. Considering that the lengthiest calculation time was made by $w = 100$, performing the algorithm took less than 1 msec for each round. Therefore, we can guarantee that our system works in real time and in a continuous state.

VII. Discussion

Regarding Fig. 4, we expect to have the total amount of distortion equal to the multiplication of 9.8%, 12.2% and 13% (i.e., 0.15%). However, the best value for the distortion probability in our system was 1.15%, which was higher than the expected value. Perhaps the reason was that we only considered low amplitude areas caused by phase interference of light as the major source of fading, while other sources, such as the state of polarization, were not considered. These other reasons deteriorated the actual value of the distortion probability compared with the expected value. The suppression of other fading sources should be further studied in future studies.

Additionally, we chose to multiply the mean amplitude values from columns *A* and *B* (*M_k1* and *M_k2* in the flowchart) because multiplication will provide us with a very fast response at the output. Nonetheless, if agility does not matter in the system, we can add more constraints at this stage, resulting in a more sophisticated algorithm.

VIII. Conclusion

We proposed a Φ-OTDR system with a continuous fading suppression ability based on optimum tracking over multiple probe frequencies. The proposed method can successfully forecast the occurrence of distortion in the output phase signal and avoid it by jumping to a better phase signal. This algorithm has a fast response, high repeatability, and real-time processing properties. We attained a distortion-free output over 98.85%, under a long time of continuous running with the proposed system, which provides a promising DAS solution for practical online purposes.

References

[1] A. Hartog *et al.*, "The use of multi-frequency acquisition to significantly improve the quality of fibre-optic-distributed vibration sensing," *Geophys. Prospecting*, vol. 66, pp. 192–202, 2018.
[2] P. Healey, "Fading in heterodyne OTDR," *Electron. Lett.*, vol. 20, pp. 30–32, 1984.
[3] H. Izumita, S.-I. Furukawa, Y. Koyamada, and I. Sankawa, "Fading noise reduction in coherent OTDR," *IEEE Photon. Technol. Lett.*, vol. 4, no. 2, pp. 201–203, Feb. 1992.
[4] H. Izumita, Y. Koyamada, S. Furukawa, and I. Sankawa, "Stochastic amplitude fluctuation in coherent OTDR and a new technique for its reduction by stimulating synchronous optical frequency hopping," *J. Lightw. Technol.*, vol. 15, no. 2, pp. 267–278, Feb. 1997.
[5] D. Chen, Q. Liu, and Z. He, "High-fidelity distributed fiber-optic acoustic sensor with fading noise suppressed and sub-meter spatial resolution," *Opt. Express*, vol. 26, pp. 16138–16146, 2018.
[6] J. Zhang, H. Zheng, T. Zhu, G. Yin, M. Liu, Y. Bai, *et al.*, "Long range fading free phase-sensitive reflectometry based on multi-tone NLFM pulse," in *Proc. 26th Int. Conf. Opt. Fib. Sens.*, Lausanne, Switzerland, 2018, Paper TuC3.
[7] A. Masoudi, M. Belal, and T. Newson, "A distributed optical fibre dynamic strain sensor based on phase-OTDR," *Meas. Sci. Technol.*, vol. 24, 2013, Art. no. 085204.
[8] G. Tu, X. Zhang, Y. Zhang, F. Zhu, L. Xia, and B. Nakarmi, "The development of an Φ-OTDR system for quantitative vibration measurement," *IEEE Photon. Technol. Lett.*, vol. 27, no. 12, pp. 1349–1352, Jun. 2015.
[9] J. Zhou, Z. Pan, Q. Ye, H. Cai, R. Qu, and Z. Fang, "Characteristics and explanations of interference fading of a ϕ-OTDR with a multi-frequency source," *J. Lightw. Technol.*, vol. 31, no. 17, pp. 2947–2954, Sep. 2013.
[10] A. Hartog, *An Introduction to Distributed Optical Fibre Sensors*. Boca Raton, FL, USA: CRC Press, 2017, pp. 88–91.
[11] X. He *et al.*, "Multi-event waveform-retrieved distributed optical fiber acoustic sensor using dual-pulse heterodyne phase-sensitive OTDR," *Opt. Lett.*, vol. 42, pp. 442–445, 2017.
[12] L. Zhang *et al.*, "Phase-sensitive optical time-domain reflectometry with I/Q demodulation," in *Proc. Asia Commun. Photon. Conf.*, 2015, Paper AM1I. 3.
[13] K. Shimizu, T. Horiguchi, and Y. Koyamada, "Characteristics and reduction of coherent fading noise in Rayleigh backscattering measurement for optical fibers and components," *J. Lightw. Technol.*, vol. 10, no. 7, pp. 982–987, Jul. 1992.
[14] A. Hartog, *An Introduction to Distributed Optical Fibre Sensors*. Boca Raton, FL, USA: CRC Press, 2017, pp. 249–254.

Mohammadmasoud Zabihi received the Master's degree in optical engineering from Nanjing University of Science and Technology, Nanjing, China, in 2017. He is currently working toward the Ph.D. degree in optical engineering at Nanjing University. His research interests are optical time-domain reflectometry, distributed optical acoustic and vibration sensing, and intrusion detection systems.

Yusheng Chen received the Bachelor's degree in electrical engineering and automation in 2017 from Nanjing University of Science and Technology, Nanjing, China, where he is currently working toward the Master's degree in the School of Automation. His research interest is distributed optical fiber sensors.

Tong Zhou received the Bachelor's degree in computer science and technology from Chongqing Jiaotong University, Chongqing, China, in 2017. She is currently working toward the Master's degree in optical engineering at Nanjing University, Nanjing, China. Her main research interest is optical signal processing.

Jingxiao Liu received the Bachelor's degree in electrical and optical engineering from Anhui University, Hefei, China, in 2018. She is currently working toward the Master's degree in optical engineering at Nanjing University, Nanjing, China. Her main research interest is optical fiber sensors.

Yuanyuan Shan received the Bachelor's degree in optical information science and technology from the University of Shanghai for Science and Technology, Shanghai, China, in 2011, and the Master's degree in optics from Guizhou University, Guiyang, China, in 2015. She is currently working toward the Ph.D. degree in the School of Electronics Science and Engineering, Nanjing University, Nanjing, China. Her research interests are in the distributed optical fiber sensors.

Zhen Meng received the Bachelor's degree in electronic information engineering from North China University of Technology, Beijing, China, in 2011. Then, he studied pattern recognition and intelligent systems at Beijing University of Posts and Telecommunications, Beijing, China, in 2012. Since 2014, he has been working toward the Ph.D. degree in control science and engineering. His research interests are distributed optical fiber sensors and data analysis.

Feng Wang received the B.S. degree in optics and Ph.D. degree in microelectronics and solid-state electronics from Nanjing University, Nanjing, China, in 2003 and 2009, respectively. He is currently with the College of Engineering and Applied Sciences, Nanjing University, where he is currently an Associate Professor. He is the author of more than 60 articles and more than 30 inventions. His current research interests are in the principles and applications of distributed optical fiber sensing, the techniques of electronic-optical detection, and signal processing.

Yixin Zhang received the B.S. and Ph.D. degrees from the University of South East, Nanjing, China, in 2006 and 2011, respectively. In 2011, he joined the Nanyang Technological University, Singapore, as a Postdoctoral Fellow. He is currently an Associate Professor with the College of Engineering and Applied Sciences, Nanjing University, Nanjing, China. His research interests include fiber-sensor-based health-monitoring technology and digital signal processing.

Xuping Zhang received the B.S., M.S., and Ph.D. degrees from the University of South East, Nanjing, China, in 1983, 1986, and 1995, respectively. She is currently a Professor with the College of Engineering and Applied Sciences, Nanjing University, Nanjing, China. Her research interests include the monitoring and fault locating of optical communication networks, novel and key devices for optical communication system, and fiber-sensor-based health-monitoring technology.

Mengmeng Chen received the B.S. degree from the Nanjing University of Science and Technology, Nanjing, China, in 2007, and the Ph.D. degree from the Nanjing University, Nanjing, China, in 2013. Since 2013, she has been a Lecture with the School of Electronic Engineering, Nanjing Xiaozhuang University, Nanjing, China. In 2018, she joined the University of Southampton, Southampton, U.K., as an Academic Visitor. Her research interests include distributed acoustic sensor, distributed fiber-sensor-based health monitoring technology, digital signal processing, and virtual instrument.